Ultra-Low Sidelobe Waveform Design via Spectral Shaping and LINC Transmit Architecture

John Jakabosky and Shannon D. Blunt
Radar Systems Lab
University of Kansas
Lawrence, KS

Thomas Higgins
Radar Division
Naval Research Laboratory
Washington, DC

Abstract—A new spectral-shaping approach is used to design jointly the amplitude window and phase of a tapered NLFM waveform. This approach can produce physical radar emissions with ultra-low sidelobes that support sufficient spectral roll-off to maintain forthcoming spectral compliance requirements. A small SNR loss is traded for a substantial reduction in range sidelobes. Further, it is demonstrated that this tapered waveform scheme can be readily combined with the linear amplification using nonlinear components (LINC) architecture to realize the small yet necessary amplitude variation while operating the power amplifiers in saturation, which may be used to realize enhanced power efficiency. Experimental measurements demonstrate range sidelobes below –80 dB with less than 0.3 dB in SNR loss.

I. INTRODUCTION

Improving the spectral containment of radar emissions is a growing concern as the radio frequency (RF) spectrum becomes increasingly congested, most notably due to the demand for bandwidth to support wireless video access by the commercial communication industry [1,2]. For this reason, radar spectrum engineering has been a driving factor behind research into waveform diversity [3-5]. For example, excellent spectral containment was demonstrated in [6,7] using windowed sinc kernel functions. However, these approaches produced significant amplitude modulation (which translates into lost energy on target) and do not address the requirement on the radar emission to possess low range sidelobes for pulse compression. That said, [6,7] did show that such an emission with amplitude modulation can be physically realized without resorting to linear amplification by employing a classical form of linear amplification using nonlinear components (LINC) known as Chiriex out-phasing [8]. More recently, spectral containment of optimized FM waveforms has been considered using windowing [9] and hardware-in-the-loop optimization comprising a 180° coupler LINC architecture [10].

Here we consider the problem of jointly constraining the emission spectrum and minimizing range sidelobes in the context of a physical radar transmitter. The key to this waveform design problem is a well-known property used in the design of nonlinear FM waveforms that states that low range sidelobes can be achieved when the signal spectrum decreases towards the band edges [11]. Interestingly, the goals of better spectral containment and lower range sidelobes are in fact complementary design metrics [12]. Here we leverage this relationship by employing an iterative spectral shaping procedure that jointly optimizes the FM waveform and

associated amplitude taper. This approach relies upon fitting the waveform to specified spectral and envelope shapes and was inspired by approaches developed for spectral notching of waveforms [13,14], the roots of which can be traced back to various sequential projection methods (e.g. [15,16]). It is shown in simulation and experimentally that this approach can produce radar emissions with extremely low range sidelobes that also provide good spectral containment. To support amplitude modulation with saturated power amplifiers, it is also shown that this emission can be readily implemented using the 180° coupler LINC architecture. While not the focus of this paper, it should be noted that the LINC approach may provide enhanced power efficiency in such cases if properly designed (e.g. through the use of power recycling).

II. SPECTRAL-SHAPING OPTIMIZATION

The waveform design scheme employed here is a generalization of the approach used in [17] that applies a spectral shaping optimization to the design of a constant amplitude, pseudo-random FMCW waveform. While the approach in [17] is geared towards the design of non-repeating nonlinear FMCW segments, here it is aimed at the design of a single pulsed waveform that supports the joint optimization of a modest amplitude taper. To produce a waveform that fits a desired spectral shape, the optimization process is initialized with a waveform that has a similar power spectral density (PSD). For instance, a Gaussian spectral shape is known to provide low range sidelobes [11]. Likewise, an initial pulse amplitude taper is selected that is consistent with the desired spectral roll-off characteristics. A Tukey window performs adequately for this initialization as its amplitude roll-off is easy to establish.

The optimization process is separated into two stages. The first stage seeks to fit the waveform to both the specified spectral shape and the amplitude taper, with the latter serving as a soft constraint to minimize SNR loss by keeping the amplitude envelope close to constant (aside from the tapered roll-off at the pulse edges). The second stage optimizes the waveform according to the spectral shape alone since the autocorrelation is only related to the power spectral density.

The first stage of the optimization process involves the iterative application of

$$r_{i+1}(t) = \mathbb{F}^{-1}\left\{ |G(f)| \exp\left(j\angle \mathbb{F}\{ p_i(t) \} \right) \right\} \tag{1}$$

and

$$p_{i+1}(t) = w(t) \exp\left(j\angle r_{i+1}(t) \right) \qquad (2)$$

where $p_0(t)$ is some initial waveform, $|G(f)|^2$ is the desired power spectral density, $w(t)$ is the desired amplitude taper, $\mathbb{F}$ is the Fourier transform, $\mathbb{F}^{-1}$ is the inverse Fourier transform, and $\angle(\bullet)$ extracts the phase of the argument. These steps are repeated I times to generate the first stage output waveform $p_I(t)$ that possesses both FM and AM attributes.

Setting $q_0(t) = p_I(t)$, the second stage comprises the iterative application of

$$q_{k+1}(t) = x(t) \odot \mathbb{F}^{-1}\left\{ |G(f)| \exp\left(j\angle \mathbb{F}\{q_k(t)\} \right) \right\}, \qquad (3)$$

where the $x(t)$ term is a rectangular window of length T that serves to limit the temporal extent of $q_{k+1}(t)$. The second stage is repeated K times to produce the final waveform $s(t) = q_K(t)$. Both stages can be efficiently implemented using FFT and IFFT processing on a General Purpose GPU (GPGPU).

As an example, consider the design of a waveform with bandwidth $B = 80$ MHz and pulsewidth $T = 1.6$ μs so the time-bandwidth product is $BT = 128$. Using a Gaussian spectral shape and a Tukey taper with the amplitude roll-off occurring within the first and last 50 ns, the waveform is optimized for $I = K = 5000$ iterations in each of the two stages. The initial waveform was derived from the $(L = 8, M = 2)$ optimized waveform from [18] that has $BT = 64$ and a peak sidelobe level (PSL) of -52 dB. This waveform was interpolated up to $BT = 128$ using polynomial fitting to obtain $p_0(t)$ used in the optimization process above.
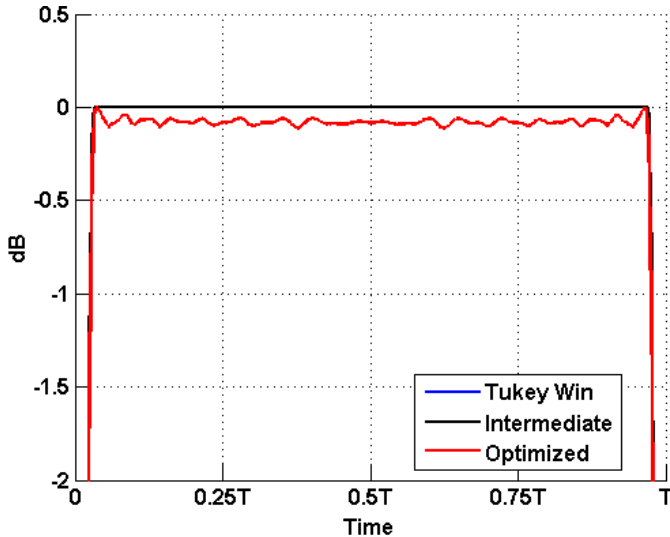
Fig. 1. Pulse envelope of optimized waveform with $BT = 128$

Figure 1 depicts the envelope for the waveform optimized via (1)-(3) where it is observed that the AM effects are rather minimal, with an associated SNR loss of only 0.26 dB. Figure 2 shows the autocorrelation of this waveform where the first stage of optimization achieves a PSL of -59.9 dB, while the final optimized waveform attains a rather astounding PSL of

-108.1 dB. Interestingly, if one were to remove the amplitude taper for the final optimized waveform more than 60 dB of degradation in PSL would result (see Fig. 2), thus illustrating the importance of this jointly optimized taper.
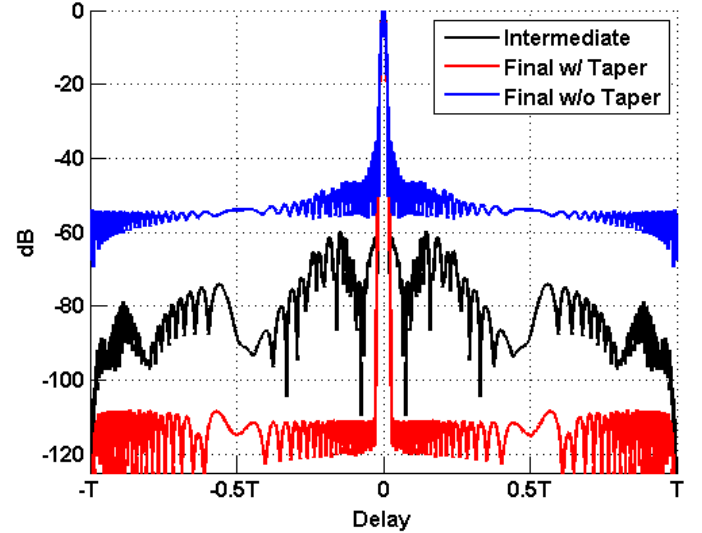
Fig. 2. Waveform autocorrelation with and without jointly optimized amplitude taper and intermediate optimization stage

The range-Doppler ambiguity function of the optimized waveform is shown in Fig. 3, where it is observed that Doppler tolerance is largely preserved with the usual Fresnel lobes indicative of NLFM waveform being present as well. Finally, Fig. 4 illustrates the spectral content of the final waveform with and without the tapering in which the lack of the optimized taper clearly degrades spectral containment as well (the intermediate and final waveform spectra lie perfectly on top of the desired Gaussian PSD).
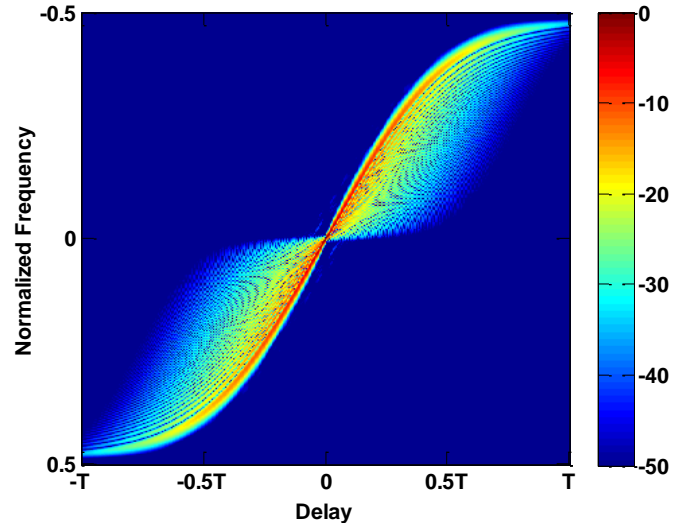
Fig. 3. Range-Doppler ambiguity function of optimized waveform
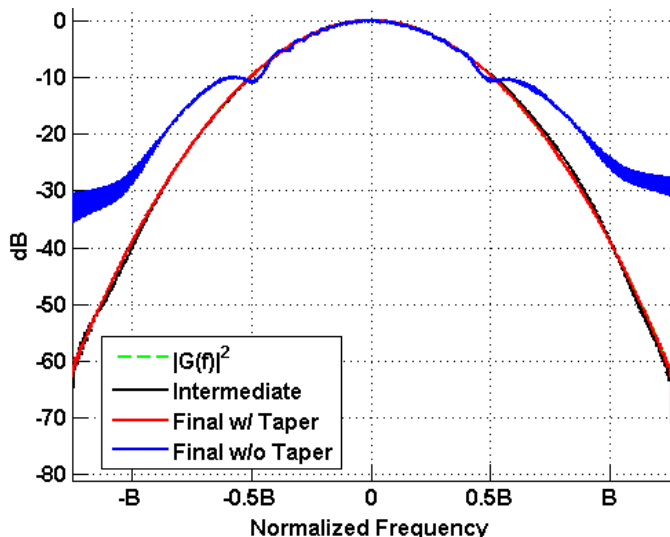
Fig. 4. Spectral content of waveform with and without jointly optimized amplitude taper

III. LINC ARCHITECTURE

While the AM attribute of the pulse, being jointly optimized with the FM component, contributes substantially to the low sidelobe level as observed in Fig. 2, the amplitude variation also complicates the physical generation of the waveform for a high-power transmitter. To avoid operating the power amplifier in the linear mode the LINC approach is considered. LINC operates by decomposing the waveform (composed of phase and amplitude as a function of time) into two constant-amplitude signals that can be separately amplified with saturated power amplifiers. The sum of these two signals produces the original waveform following this amplification. The approach used is similar to that in [10] except that the phase perturbation here is balanced between the two channels.
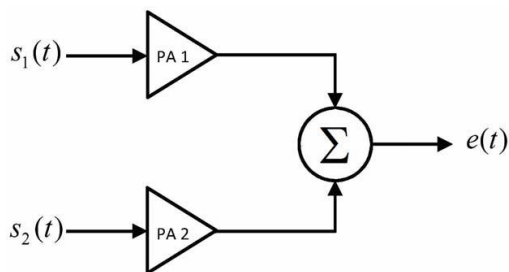
Fig. 5. LINC transmitter implementation

As shown in Fig. 5, the two signals are driven into two separate (saturated) power amplifiers and then summed using a 180° hybrid coupler or magic tee. The difference port of the coupler (not shown) is connected to a dummy load (or could be used to recycle power or for another purpose such as generating dual-polarized emissions [19]). The two signals are decomposed from the desired waveform by first determining

$$\phi(t) = \cos^{-1}|s(t)| \qquad (4)$$

so that the two signals can be expressed as

$$s_1(t) = \frac{s(t)}{|s(t)|} e^{j\phi(t)} \qquad (5)$$

and

$$s_2(t) = \frac{s(t)}{|s(t)|} e^{-j\phi(t)} . \qquad (6)$$

The $\phi(t)$ term is the phase perturbation that generates the amplitude variation of waveform $s(t)$ when $s_1(t)$ and $s_2(t)$ are combined. The physical emission generated by the LINC transmitter is thus

$$e(t) = s_1(t) + s_2(t) , \qquad (7)$$

which ideally is a scaled copy of the original waveform $s(t)$. In reality, how well $e(t)$ replicates $s(t)$ depends on the quality of the coupler's sum channel and the gain match between the two power amplifiers.

IV. EXPERIMENTAL EVALUATION

To evaluate if these ultra-low sidelobe waveforms can be achieved in practice, the optimized waveform from Sect. II was implemented on an RF testbed comprised of a Tektronix AWG70002 waveform generator and a Rohde & Schwarz spectrum analyzer. The waveform generator was used as a trigger source and the spectrum analyzer provided a 100 MHz reference for clock stability. The waveform was upsampled to 6.125 GS/s and upconverted to a center frequency of 1.8425 GHz. The spectrum analyzer was used to capture complex I and Q samples at 200 MS/s. For the responses to be visible below the noise floor, 10^4 pulses were captured and averaged.

Measurements were made for the optimized waveform being generated directly by the AWG (denoted as 'Measured') and for the waveform generated via the hybrid coupler LINC implementation (denoted as 'Measured w/ LINC'). To avoid addressing the cross-calibration of the separate power amplifiers, the LINC scheme here is driven directly by separate channels of a two-channel AWG with no intermediate power amplifiers. This amplifier cross-calibration sensitivity for waveform implementation/design was recently discussed in [10] and is a topic of continued investigation in relation to waveform optimization.

Figure 6 illustrates the matched filter response (using the filter corresponding to the optimized waveform) to each of the measured waveforms in loopback. While there is clearly some degradation relative to the ideal optimized case (that achieves a PSL of −108 dB), the sidelobes are still extremely low. Figure 7 highlights the region around the mainlobe where an asymmetric response is observed. It was determined that these one-sided shoulder lobes were due to linear artifacts (non-flat gain over the passband) in the spectrum analyzer and the LINC hybrid coupler (their removal via linear calibration will be subsequently demonstrated).
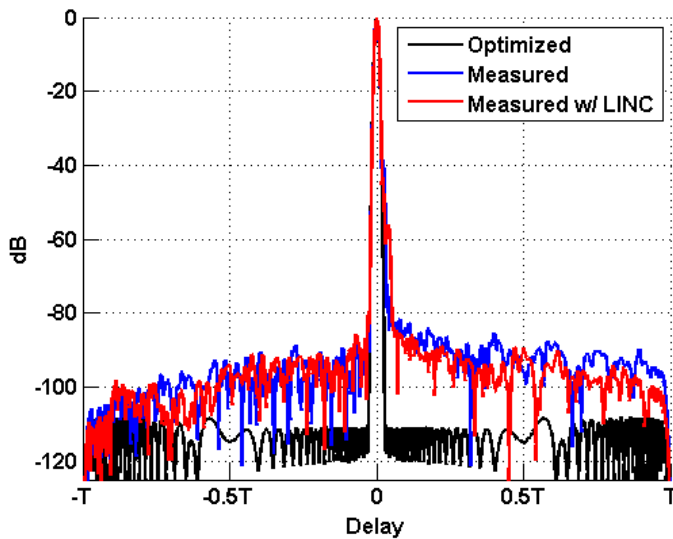
Fig. 6. Matched filter response for loopback measured waveforms
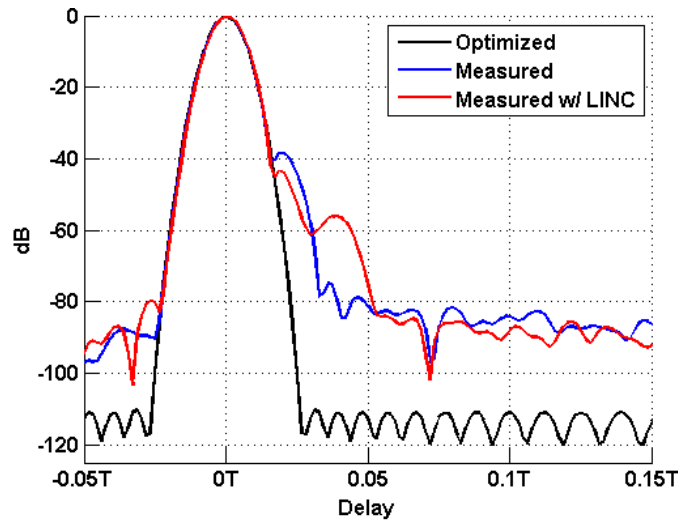
Fig. 7. Matched filter response (mainlobe detail)
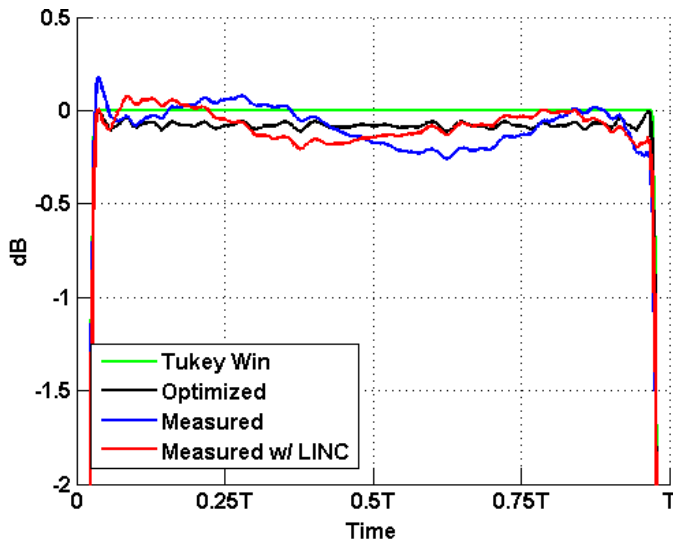
Fig. 8. Pulse amplitude envelope for loopback measured waveforms

The amplitude envelope for the two measured cases is shown in Fig. 8. While these envelopes appear to be different, if one examines the fine detail it is rather similar between the two measured and the optimized waveforms. The differences are again due to linear artifacts that will be addressed shortly. Figure 9 depicts the spectral content of the measured waveforms which match quite well with that of the optimized waveform. The slightly increased rolloff at the edge of the band are from the 160 MHz analysis bandwidth available in the spectrum analyzer.

Using Least-Squares estimation to determine and subsequently compensate for the linear artifacts generated by the spectrum analyzer and LINC architecture, the true realizable impact of this waveform optimization scheme is observed. Figure 10 depicts the measured pulse envelopes after linear compensation where the similarity is now evident. Further, Fig. 11 shows the compensated matched filter responses in which the measurements match the ideal optimized waveform to the limit of quantization error.
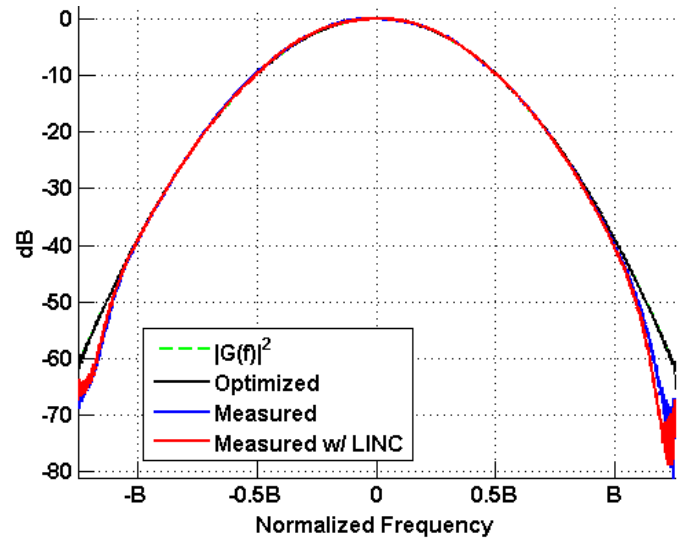
Fig. 9. Power spectral density of loopback measured waveforms
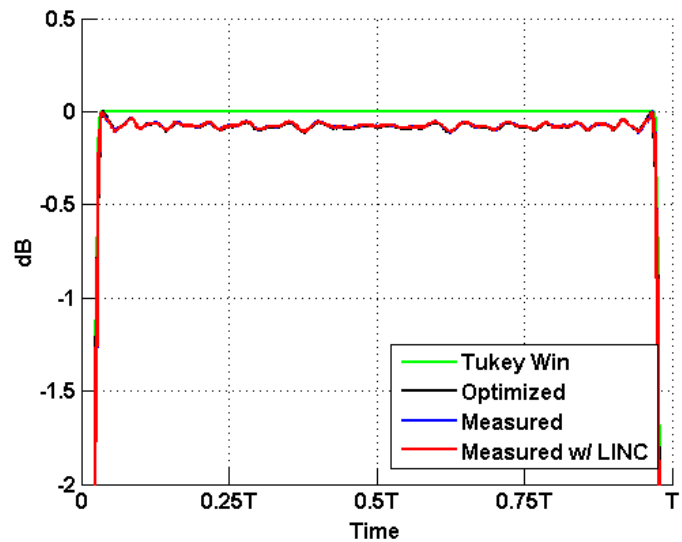
Fig. 10. Pulse amplitude envelope of the compensated measured waveforms
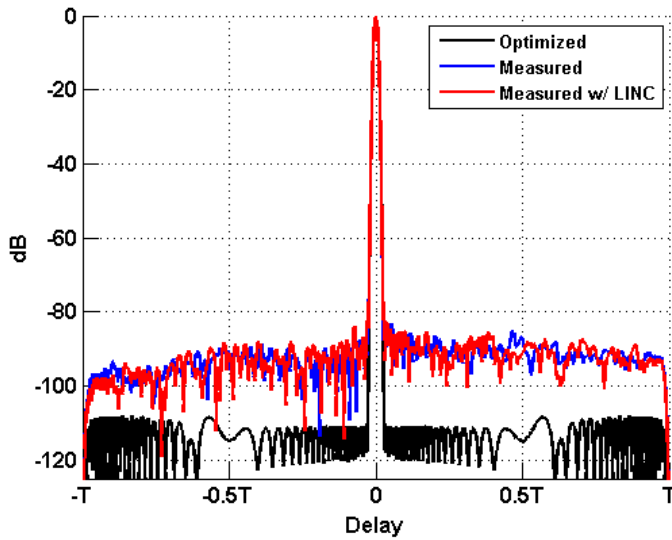
Fig. 11. Matched filter response of the compensated measured waveforms

TABLE I. MEASURED PERFORMANCE

	Init. [15]	Opt.	Meas.	Meas. LINC	Comp. Meas.	Comp. Meas. LINC
PSL (dB)	−52.0	−108.1	−74.6	−79.6	−83.2	−81.8
ISL (dB)	−36.9	−99.0	−79.1	−80.4	−81.4	−80.4
HPW (vs. LFM)	1.26	1.28	1.28	1.29	1.28	1.28
SNR Loss (dB)	0	0.26	0.27	0.29	0.26	0.26
Design BT	64	128	128	128	128	128

Table 1 compares the performance for the initial, optimized, measured, and compensated measured waveforms. Compensation reveals that the true measured PSL values are within roughly 25 dB of the ultra-low performance of −108 dB realized by the optimized waveform. This remaining difference is due to the 10-bit resolution provided by the AWG. The half-power width (HPW) measurement compares the 3 dB mainlobe width with the benchmark LFM waveform to denote the relative range resolution, which is slightly less than a 30% increase for all waveforms (and which is typical for NLFM).

To evaluate the performance of the waveform in a real environment, the waveform was emitted in an open-air experiment. For this test, the waveform was given a 1.6 µs pulse length that yielded an approximate bandwidth of 80 MHz. A center frequency of 2.3 GHz was chosen. The vertical channel of two quad-ridged horn antennas were used for transmit and receive. Each antenna provided approximately 10 dBi of gain. The Tektronix AWG70002 and Rohde & Schwarz spectrum analyzer were again used. An estimated transmit power of 22 dBm was provided by a single amplifier with 27 dB of gain. The test did not incorporate LINC since no hybrid

coupler was available at the frequency required at the time of the test. Further, the captured results of the loopback test demonstrated that the LINC approach has similar fidelity to direct generation with the AWG. A PRF of 100 kHz was used since the low transmit power prevented any significant range folding. A high PRF also allowed a high level of noise suppresion during coherent integration. A total of 1 second of data was integrated for 50 dB of coherent integration gain.

Fig. 12. Equipment used for rooftop measurements
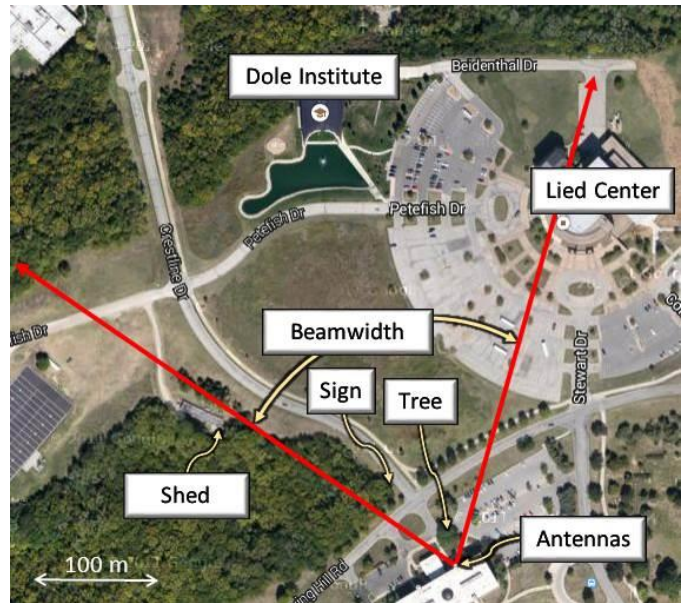
Fig. 13. Annotated map of radar scene

The test equipement was placed on the roof of a 3 story building located at the University of Kansas as shown in Fig. 12. The antennas were aimed at the Dole Institute at a range of approximately 360 meters. The spatial arrangement of possible scatterers are shown in Fig. 13. The matched filtered and coherently integrated range profile estimate is shown in

Fig. 14. The scatterers labeled in Fig. 13 are annotated at their ranges in Fig. 14. The pulse width of the waveform is also shown in Fig. 14. The sidelobe floor of this waveform prevents the direct path from obscuring small targets during the transmission interval of 1.6 µs or 240 meters. An apparent dynamic range of greater than 70 dB is available while the transmitter is active.
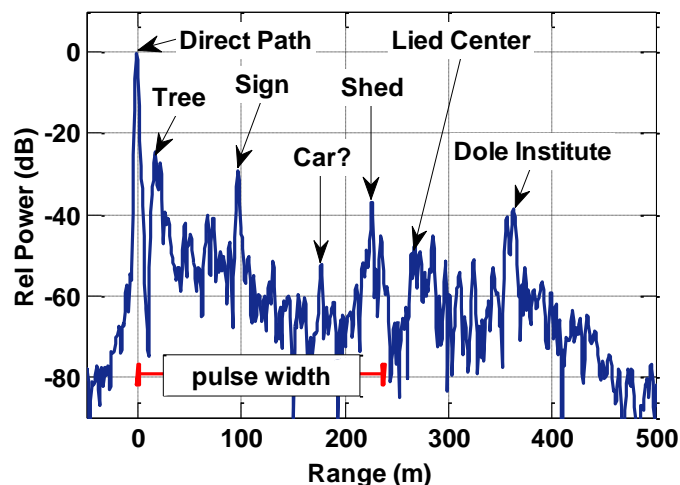
Fig. 14. Annotated range profile showing pulse width

V. CONCLUSIONS

An ultra-low sidelobe waveform design scheme, achieving a measured PSL better than –80 dB and with roughly a quarter dB in SNR loss has been demonstrated. This approach relies upon spectral shaping optimization to design jointly the FM component of the waveform and the low-loss amplitude taper. This type of waveform was shown to be implementable using a hybrid coupler in LINC configuration as a means to provide linear amplification. The performance of the waveform was also demonstrated with an open-air experiment. Ongoing work includes applying the spectral shaping optimization with different spectral and time window shapes.

REFERENCES

[1] H. Griffiths, S. Blunt, L. Cohen, and L. Savy, "Challenge problems in spectrum engineering and waveform diversity," *IEEE Radar Conf.*, Ottawa, Canada, 29 Apr. – 3 May 2013.

[2] H. Griffiths, L. Cohen, S. Watts, E. Mokole, C. Baker, M. Wicks, and S. Blunt, "Radar spectrum engineering and management: technical and regulatory issues," to appear in *Proc. IEEE*.

[3] M. Wicks, E. Mokole, S. Blunt, R. Schneible, and V. Amuso, eds., *Principles of Waveform Diversity and Design*, SciTech, 2010.

[4] U. Pillai, K.Y. Li, I. Selesnick, and B. Himed, *Waveform Diversity: Theory & Applications*, McGraw-Hill, 2011.

[5] F. Gini, A. De Maio, and L.K. Patton, eds., *Waveform Design and Diversity for Advanced Radar Systems*, IET, 2012.

[6] R. Chen and B. Cantrell, "Highly bandlimited radar signals," *IEEE Radar Conf.*, Long Beach, CA, pp. 220-226, Apr. 2002.

[7] H. Faust, B. Connolly, T.M. Firestone, R.C. Chen, B.H. Cantrell, and E.L. Mokole, "A spectrally clean transmitting system for solid state phased-array radars," *IEEE Radar Conf.*, Philadelphia, PA, pp. 140-144, Apr. 2004.

[8] H. Chiriex, High power outphasing modulation," *Proc. IRE*, pp. 1370-1392, Nov. 1935.

[9] S.D. Blunt, M. Cook, E. Perrins, and J. de Graaf, "CPM-based radar waveforms for efficiently bandlimiting a transmitted spectrum," *IEEE Radar Conf.*, Passadena, CA, 4-8 May 2009.

[10] L. Ryan, J. Jakabosky, S.D. Blunt, C. Allen, L. Cohen, " Optimizing polyphase-coded FM waveforms within a LINC transmit architecture," *IEEE Radar Conf.*, Cincinnati, OH, pp.835-839, 19-23 May 2011.

[11] J.A. Johnston and A.C. Fairhead, "Waveform design and Doppler sensitivity analysis for nonlinear FM chirp pulses," *IEE Proc. F – Communications, Radar & Signal Processing*, vol. 133, no. 2, pp. 163-175, Apr. 1986.

[12] S.D. Blunt, J. Jakabosky, M. Cook, J. Stiles, S. Seguin, and E.L. Mokole, "Polyphase-coded FM (PCFM) radar waveforms, part II: optimization," *IEEE Trans. Aerospace & Electronic Systems*, vol. 50, no. 3, pp. 2230-2241, July 2014.

[13] T. Higgins, T. Webster, and A.K. Shackelford, "Mitigating interference via spatial and spectral nulls," *IET Intl. Radar Conf.* , 22-25 Oct. 2012

[14] W. Rowe, P. Stoica, and J. Li, "Spectrally constrained waveform design," *IEEE Signal Processing Magazine*, vol. 31, no. 3, pp.157-162, May 2014.

[15] A. Levi and H. Stark, "Image restoration by the method of generalized projections with application to restoration from magnitude," *J. Opt. Soc. Am.*, vol. 1, no. 9, pp. 932-943, Sept. 1984.

[16] O.M. Bucci, G. Franceschetti, G. Mazzarella, and G. Panariello, "Intersection approach to array pattern synthesis," *IEE Proc. H – Microwaves, Antennas and Propagation*, vol. 137, no. 6, pp. 349-357, Dec. 1990.

[17] J. Jakabosky, S.D. Blunt, and B. Himed, "Waveform design and receive processing for nonrecurrent nonlinear FMCW radar" *IEEE Intl. Radar Conf.*, Washington, DC, 11-15 May 2015.

[18] J. Jakabosky, S.D. Blunt, B. Himed, " Optimization of "over-coded" radar waveforms," *IEEE Radar Conf.*, Cincinnati, OH, pp.1460-1465, 19-23 May 2011.

[19] P. McCormick, J. Jakabosky, S.D. Blunt, C. Allen, and B. Himed, "Joint polarization/waveform design and adaptive receive processing," *IEEE Intl. Radar Conf.*, Washington, DC, 11-15 May 2015.